Arabian Journal of Geosciences (2021) 14: 1233
https://doi.org/10.1007/s12517-021-07528-y

ORIGINAL PAPER

Origin of deep-water sediment wave fields in the Northern Continental Slope, South China Sea

HaiRong Wang[1,2] · ChengQian Yu[1,2] · Zhipeng Huo[1,2]

Received: 9 June 2020 / Accepted: 3 June 2021 / Published online: 23 June 2021
© Saudi Society for Geosciences 2021

Abstract

A study utilizing a dense grid of seismic and piston-core data revealed that four different types of sediment wave fields have formed on the northern slope of the strongly enclosed and low-latitude marginal South China Sea (SCS). Their origins include turbidite flow, bottom current, gravity-induced deformation, and multi-origin. Three sediment wave fields formed by turbidite flow are neighboring to the channel or canyon, have the up-current migration and decreased size from a shallow depth to deeper water, have greater content of sand and decrease of grain size from upslope to downslope, and a lower content of $CaCO_3$. Bottom current's sediment wave fields are parallel to the slope, with small-size erosive troughs, scours or furrows, and convex depositional system on the downslope of the erosive field, and with a lower content of sand, a finer grain size, and a greater content of $CaCO_3$. Gravity deformation's sediment wave fields are adjacent to the canyon, and develop several sliding surfaces corresponding to wave troughs, wave variation of no regularity. One sediment wave field was more symmetrical, displayed a smooth and rounded morphology, and has not evident migration direction, which is the result of the interaction of turbidite flows and bottom currents. Every sediment wave field involves a complex interaction between geomorphology, tectonic setting of neighboring area, and oceanography of the SCS. This study assists us to understand deeply the sedimentation processes and correspondingly depositional system in the deep-water with strongly enclosed and low-latitude characteristics and analyze the context and propagation direction of the arc-continent between the Eurasian Continent and the Luzon Arc.

Keywords Sediment waves · Turbidite flow · Bottom current · Gravity deformation · South China Sea

Introduction

Deep-water sediment waves are common in the seafloor bedform, and have been reported by many scholars from numerous marine settings, especially on slopes and rises (Damuth 1979; Faugéres and Stow 1993; Wynn et al. 2000; Cattaneo et al. 2004; Jallet and Giresse 2005; Casalbore et al. 2014; Casalbore et al. 2020; Droghei et al. 2016; Ribo et al. 2018; Alexandre et al. 2019). These deep-water bedforms are typified by multiple wave-forming processes, which controls or influences the corresponding responses of sedimentation and the accumulation of complex depositional systems (Faugères et al. 1999; Wynn and Stow 2002; Chen et al. 2017). Turbidite current and bottom current sediment waves present waveform's migration, whereas those wavy bedforms generated by gas seepage, shear sliding, and gravity deformation are not migrated (Lee and Baraza 1999; Lee et al. 2002; McCave 2017). In many cases, wave bedforms are developed by a complex interaction of multiple processes, and their initiation and evolution require precise analysis (Howe 1996; McCave 2017; Warratz et al. 2019).

Bottom current sediment waves usually refer to those formed by both geostrophic and non-geostrophic currents and, in most cases, the geostrophic downslope currents which roughly parallel bathymetric contour. Bottom currents have been recognized as the mechanisms to form sediment waves in the Barra Fan of the Rockall Trough in the northwestern United Kingdom (Knutz et al. 2002), Argentine Basin (Von

Responsible Editor: Attila Ciner

✉ HaiRong Wang
245098254@qq.com

✉ Zhipeng Huo
huozhipeng521@163.com

[1] School of Energy Resources, China University of Geosciences, Beijing 100083, China

[2] Key Laboratory for Marine Reservoir Evolution and Hydrocarbon Abundance Mechanism, Ministry of Education, China University of Geosciences, Beijing 100083, China

Lom-Keil et al. 2002; Warratz et al. 2019), the Caroline Basin (Baldwin et al. 2017), the Gulf of Valencia margin (Ribó et al. 2016a, b), and offshore eastern Canada (Normandeau et al. 2019). Bottom current sediment waves contain abundant information for palaeoceanography and regional tectonic evolution. The initiation and evolution of deep-water exchange between the northern Atlantic and Norwegian Sea was established through the analyses of contourite drift, including contourite sediment waves (Wright and Miller 1996; Stoker 1998; Davies et al. 2001). The contourite drift includes abundant bottom current pathways and seismic information about current intensity changes.

Turbidite sediment waves are commonly components of turbidite systems, and occur in submarine valleys, in particular those related to overbank depositional elements (Fildani et al. 2006; Casalbore et al. 2018). Coarse-grained sediment waves, composed of gravels and sands, have developed on the submarine slopes on the seafloor of the Eastern Valley of the Laurentian Fan (Wynn et al. 2002). The turbidite sediment waves of the Var Sedimentary Ridge exhibit classic migrating characteristics (Migeon et al. 2000; Jorry et al. 2011). Fine-grained sediment waves of mainly clay and silt are more widespread than coarse-grained sediment waves, and are recorded in the Monterey Fan (Normark et al. 1980; Normark et al. 2002; Klauckea et al. 2004). These sediment wave fields are the depositional sites for entraining material of turbidite flows that overflow the channels (Khripounoff et al. 2003). The distribution of turbidite sediment wave fields is thought to be more limited, with sizes of mostly tens or hundreds of square kilometers (Wynn et al. 2000; Ercilla et al. 2002a, b; Normark et al. 2002;Migeon et al. 2004; McCave 2017). Additionally, turbidite sediment waves can reveal information about provenance and regional tectonics. Sedimentary deformation also form wave-like bedforms, which have been ascribed as one type of sediment wave (O'Leary and Laine 1996; Mulder and Cochonat 1996; Faugères et al. 1999; Gardner et al. 1999; Ercilla et al. 2019). However, many wave fields form as a result of the interaction of multiple processes. The sediment wave field of Landes Plateau in the Bay of Biscay has been inferred to be compressional ridges resulting from deformation associated with a slump (Kenyon et al. 1978). Faugères et al. (2002) reinterpreted the origin of the Landes Plateau sediment wave field as being caused by the interaction of depositional and gravity deformation processes.

Several scientists have summarized the diagnostic features and classification criteria for three kinds of sediment waves (Wynn et al. 2000; Lee et al. 2002; Faugères et al. 2002; Cattaneo et al. 2004; Berndt et al. 2006; Ercilla et al. 2019). These criteria are used in this study (Table 1).

The understanding of the origin and evolution of sediment waves, including their initiation, construction, architecture, and even destruction, may be a key to reconstruct deep-water depositional processes, pathways, and their interactions. The wave-

Table 1 Summarization of diagnostic criterion of three types of sediment waves including bottom current sediment wave, gravity flow sediment wave, and waves of soft sediment deformation (Lee et al. 2002; Faugères et al. 2002; Wynn et al. 2000; Berndt et al. 2006; Cattaneo et al. 2004)

Wave type	Migration style	Dimensions	Geometric variability	Sediment	Process	Location
Gravity flow sediment waves	Upslope and upcurrent migration	Wave dimension progressively decrease downslope	In cross section, the overall field exhibit concave-upward surface	Turbidities, interbedded with marls, clays and oozes	Mainly turbidity flow	Slopes of volcanic islands and seamounts, levee backslopes, channel floors.
Bottom current sediment waves	Upslope migration and downcurrent migration	Wave dimension decrease in near the edge of wave fields	More larger, more nearer the center of current, usually the moats	Interbedded fine-grained silts, clays, marls and oozes	Bottom current	Parallel to bathymetric contours, on the continental margin, around seamounts and oceanic basin
Soft sediment deformation, waves	No migration	Varied dramatically	Exhibits no regularity	Muddy to sandy sediments	Creeping, sliding, slumping and occasionally compaction	Steep to gentle slopes (continental slopes, volcanic seamounts)

like bedform on the slope of the Cadiz Gulf also was once considered to be the result of landslides (Lee and Baraza 1999). The SCS is the largest marginal sea of the Western Pacific, and it is strongly enclosed. There is water mass exchange between the northeastern SCS and the Western Philippine Sea through Luzon Strait, but the types and characteristics (pathway, depth and area) of sediment waves, and their origins are not fully understood (Qu 2002; Centurioni et al. 2004; Chang et al. 2010; Lan et al. 2013; Chen et al. 2017). Furthermore, the SCS is located in an area of low latitude. Studies on the exchange of deep-water and thermohaline circulation have been focused on the North Atlantic, Central Scotia Sea, Okhotsk Sea, and other oceans neighboring the Antarctic, and are all high-latitude and open oceans (Davies et al. 2001; Wong et al. 2003; Maldonado et al. 2003; Masson et al. 2004; MacLachlan et al. 2008; Schlüeter and Uenzelmann-Neben 2008). In addition, other studies in mid-latitude and open oceans have been conducted in the Gulf of Cadiz, which is influenced strongly by the Mediterranean Outflow Water, and the Gulf of Mexico, which is swept by the Loop Current, and the Campos Basin, which is swept by northward-flowing currents (Southern Ocean Current) (Habgood et al. 2003; Llave et al. 2006; Viana et al. 2007; Petrovic et al. 2019).

Therefore, the aim of this study is to investigate sedimentary wave fields recognized in the strongly enclosed and low latitude SCS. By this, we provide insights on the features and origins of these sediment waves. This will help us understand the sedimentation processes and correspondingly depositional system in the strongly enclosed and low-latitude marginal sea, which is influenced by propagation of the arc-continent between the Eurasian Continent and the Luzon Arc.

Geologic setting

The SCS is one of the low-latitude and largest marginal sea areas in the Western Pacific Ocean, covering an area of 3.5 × 10^6 km^2. It is strongly semi-enclosed (Wang 1999) because of

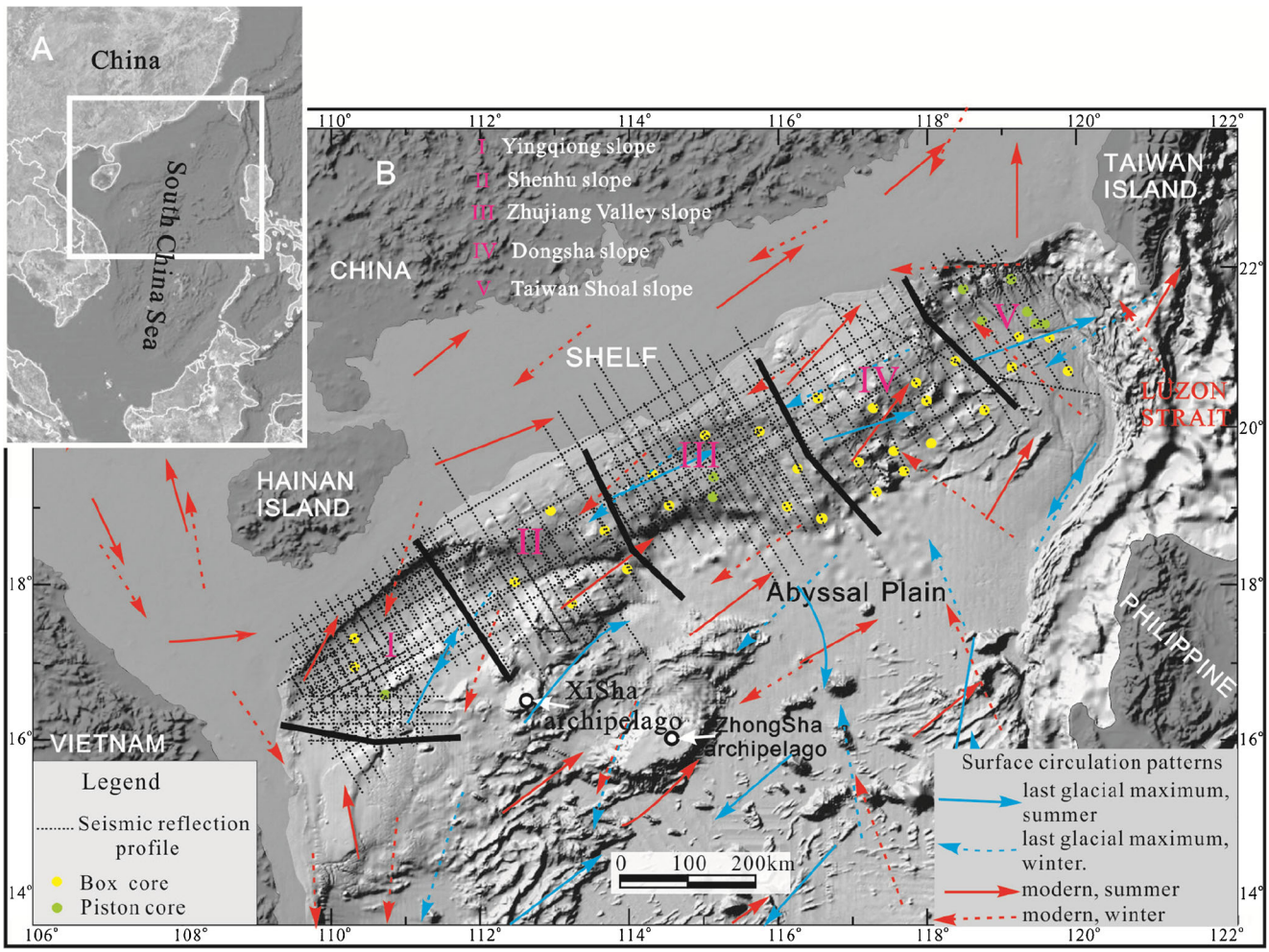

Fig. 1 (A) Map showing location of the South China Sea (study area indicated on inset map). (B) Bathymetry of the northern margin of the South China Sea (SCS), along its northern slope is divided into the Ying-Qiong slope, Shenhu slope, Zhujiang Valley slope, Dongsha slope, and Taiwan Shoal slope, respectively indicated by I, II, III, IV, V (Wang 2007). Surface circulation patterns are shown (Wang et al. 1995). The seismic grid collected over several years, and cores taken in this study, are also shown

the Taiwan orogeny, which was the result of oblique collision of the Luzon Arc with the Eurasian continent from the Late Miocene to present (Suppe 1981; Ho 1988; Lin et al. 2003). Due to the oblique nature of the collision and corresponding southward propagation of the collision focus (Huang et al. 2000), the Taiwan Island exhibit high relief and strong denudation, the rate of which can attain 1300 mg/cm^2·a in the Central Mountain area (Li 1976). This relief and erosion also is propagating southward.

The northern slope of the SCS can be divided into five units: the Yingqiong, Shenhu, Zhujiang Valley, Dongsha, and Taiwan Shoal slopes, respectively (Wang et al. 2008). All these segments differ greatly in their characteristics (Fig. 1), such as distinct tectonic histories, and unique systems of clastic sedimentary supply and dispersal. The Shenhu, Zhujiang Valley, and Taiwan Shoal slope all have host wave-like bedforms. The Shenhu slope is W-E striking, and the western segment is steeper than the eastern segment. The Zhujiang Valley slope is an enormous NW-SE valley, which links the shallow shelf to the abyssal plain at 3700 m of water depth. This slope exhibits a characteristic geomorphology of steep upper slope, gently smooth mid-slope, and steep lower slope. The Taiwan Shoal slope is different from those mentioned above and is formed by slides and slumps processes, and a slope break is developed at the toe of the slump, where slope is gradually incorporated into the Manila trench.

There are several large rivers supplying an enormous and continuous amount of terrigenous clastics to the shelf, and eventually to the slope driven by the down-slope transporting processes on the northern margin. The Pearl and Han rivers in Chinese mainland supply large amounts of clastic materials to the Shenhu and Zhujiang slopes. The Tsengwen Hsi and Kaoping Hsi rivers of the Taiwan Island discharge large amounts of clastics to neighboring deep-water environments and the Taiwan Shoal slope through the Shoushan and Gaoping canyons. Additionally, slopes around Dongsha Island also can transport carbonate clastics to the neighboring Dongsha and Taiwan Shoal slopes under gravity-flow processes. All of these down-slope processes ensure a continuous supply of material for deep-water sedimentation and formation of sediment waves.

The only possible passage of deep-water exchange with the ambient open ocean, referred to as the Western Philippine Sea, is the so-called Luzon Strait (Li et al. 1998; Su 2004), which is located on the northeastern side of the SCS and has a sill depth of about 2400 m (Fig. 1). The water mass of the Western Philippine Sea (WPS) or Kuroshio Current intrude the neighboring north slope of the SCS. The activity of corresponding bottom currents deeply influences deep-water sedimentation of these areas, which includes transportation of pre-existing clastic materials through tractive currents, formation of erosive or constructive features, and accumulation of sediment drift (Shaw 1991; Metzger and Hurlburt 1996, 2001; Li et al. 1998; Su 2004). These processes interact with down-slope processes and form more complex depositional systems. In addition, the Penghu Canyon is one important sediment-transporting passage to the south, and also exhibits migration southwestward and transports plenty of clastics towards deep water environments to the south. This is aided by the numerous gullies and canyons, which have developed on the Kaoping Slope of SW Taiwan (Fig. 2).

There are three identified currents or gyres influencing the upper ocean of the northern SCS. They are (1) the quasi-seasonal component of wind forcing; (2) the net water transport into the SCS through Luzon Strait (Su 2004); and (3) the vorticity advection from the Kuroshio, which has an oscillating characteristic and also induces meso-scale eddies (Liu and Su 1992; Su 1998). Additionally, the intensified western boundary current of the cyclonic gyre, called the Dongsha Current, flows southwestward next to the shelf south of China (Scsio 1985; Su 2004). Meso-scale eddies from the SCS basin sometimes bathe the slope area. A persistent northeastward South China Sea Warm Current (SCSWC) straddles the shelf-break region (Guan 1978).

Materials and methods

This study is based on bathymetry, piston cores, and seismic reflection profiles (Fig. 1). Regional bathymetric maps with low resolution were only used for regional morphological investigations and establishment of the interrelationship between sediment wave fields and geomorphological elements, such as canyon, terrace, and slope. Additionally, many piston cores ranging in length from 1 to 12 m, and many box cores were collected (green and yellow point in Fig. 1). Cores were split, photographed, and visually described. All cores were sampled for bulk grain size at average intervals of 20 cm. Grain-size (including median grain size) analyses of selected core units were performed using a Mastersizer 2000 laser granulometer. The percent of $CaCO_3$ and organic carbon content also were acquired in core HD-77 at the same intervals. Sedimentological analysis (e.g., grain size, facies, components, X-ray imagery) of related cores was performed in order to characterize differences among the wave fields. Seismic reflection profiles were acquired from 2002 to 2009, using Sleeve Gun I working at a 1-ms sample interval. High-resolution single-channel seismic profiles associated with 3.5 kHz echo-sounder lines also were incorporated. The trace interval was 40 m and the sonic velocity of seawater was 1500 m/s. The detailed study of the architecture, geometry, and stratigraphy of sediment wave fields is based mainly on seismic profile analyses. The parameters on wave-length (WL) and wave-height (WH) can be attained from the seismic profile through calculations of the two-way time and sonic velocities of seawater. The WL is the crest-to-crest or trough-to-

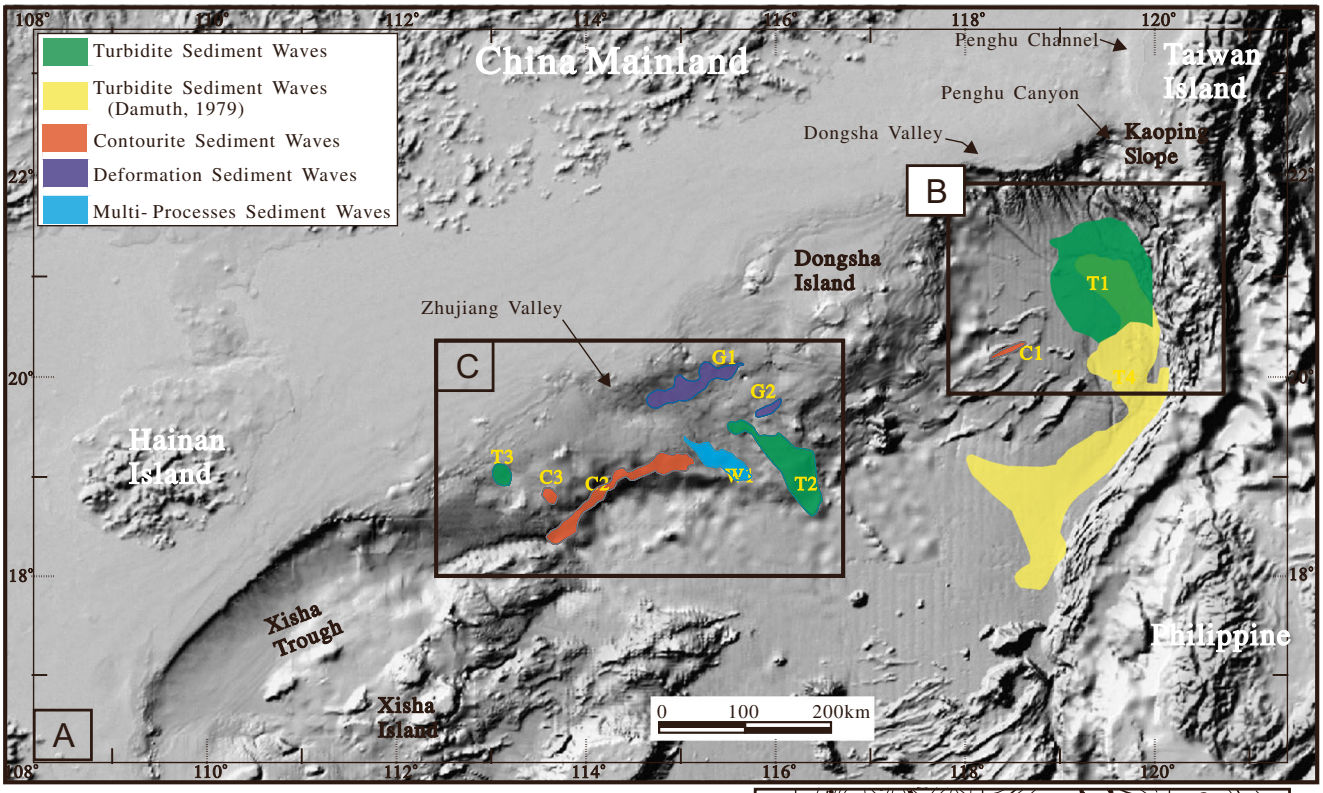

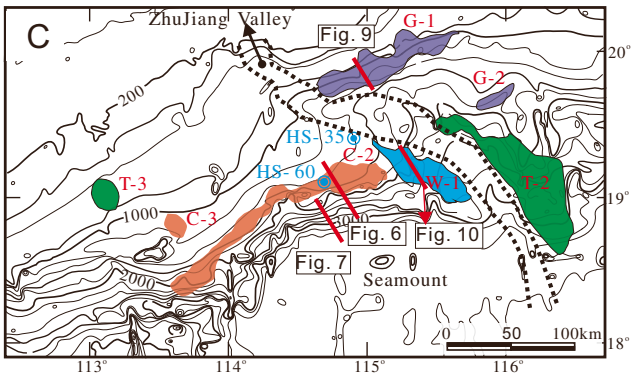

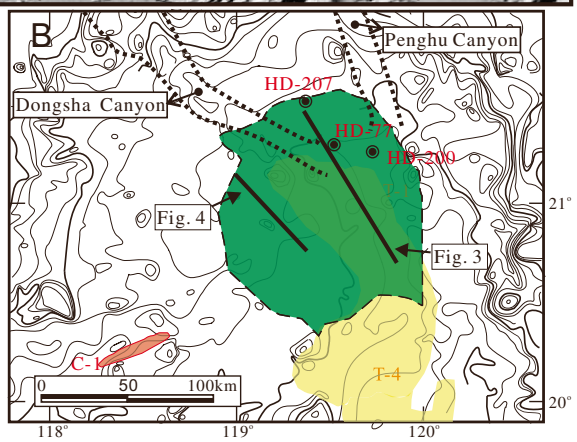

Fig. 2 (A) Sediment waves fields of different origin are illustrated for the slope of the northern margin of the South China Sea. Two inset maps locate sites B and C. (B) Turbidite wave field T-1 and part of T-4 are illustrated clearly, and important morphosedimentary elements, such some canyons also are shown. (C) Three types of wave, including those of contourite, multi- and deformational origin, are listed on the detailed geomorphological map. Seismic profiles and cores discussed in the text are illustrated in B and C. The scale, location, and other features of every wave field are listed in Table 2

trough distance, and the WH is the height of crest to trough. Based on the interpretation of every profile, the distribution of every wave field can be drawn and the trend of these fields was analyzed one by one according to the location and inter-relationship with other geomorphological elements.

Results and discussion

Four sediment wave fields were discerned on the northern slope of the South China Sea based on characteristics and the approximate geomorphology on the map (Fig. 2A).

Turbidite sediment wave fields

Characteristics

Three similar sediment wave fields, indicated with green shading (T-1, T-2, and T-3) in Fig. 2, were recognized on the northern slope of the SCS (Fig. 2A). The parameters of these fields are listed in Table 2. Furthermore, a large field of migrating sediment waves (T4, yellow shading in Fig. 2) covering an area of about 25,000 km^2 was drawn on the western wall of the Manila Trench (Wang et al. 2008; Gong et al. 2012), which was discovered by Damuth (1979) based on

Table 2 Location, size, annotation, and some interpretation of the sediment wave fields in the northern continental margin of the South China Sea

Types of sediment wave	Color	Code name	Location	Size of wave fields (km2)	Wave length (m)	Wave height (m)	Wave length/ wave height	Other remarks
Turbidite sediment wave fields	Green	T-2	Eastern flank of the Zhujiang Valley, located in the lower slope	3640	2800	14	200	
		T-3	Middle slope of the Shenhu offshore	430	750	9	83	
		T-1	Northern part of the Manila Trench, also the Taiwan Shoal Slope	12500	4300	26	165	The overlapping area of two wave fields is about 2890 km^2, and constitutes the extensive field of about 35000 km^2.
		T-4	Discerned by Damuth (1979)	25000				
Contourite sediment wave fields	Red	C-1	Lower slope of the southeastern flank of the Dongsha Slope Segmentation	263	360	16	23	The size of contourite sediment wave fields is little in general, and differs dramatically between them.
		C-2	The transition of middle slope to lower slope of Shenhu Region	2707	1820	69	26	
		C-3	The middle slope of Shenhu Region	240	280	16	18	
Deformation wave fields	Purple	G-1	The upper and middle slope of Shenhu Region, adjoining to Zhujiang Valley	1940	1400	73	19	Its distribution is correlated with those gigantic deep-water canyons.
		G-2	The southwestern flank of Dongsha Island, adjoining canyon	259	480	29	17	
Sediment wave fields of multiple origin	Blue	W-1	Middle and lower slope, located on the western and southern flanks	1387	3000	33	91	Influenced by bottom current and gravity flows simultaneously.
		W-2	Middle and lower slope of Xisha Trough	2350	3600	27	133	Influenced by gravity and bottom current.

utilization of 3.5-kHz echogram profiles (Fig. 2). This site is termed "Taiwan Shoal Slope" in this study.

The multiple-channel seismic profile in Fig. 3 illustrates the characteristics of the sediment wave field (T-1), which occupies an extensive region of 12,500 km^2 and includes an overlapping area of 2890 km^2 with Damuth's (1979) wave field. These combined areas constitute an extensive wave field of 35,000 km^2.

The thickness (two way travel time, TWT) of the sequence of waveform ranges from 220 to 410 ms (Fig. 3). The upslope and downslope flanks of the sediment wave exhibit conspicuous differences in wave thickness and flank length. The thickness of the upslope flank shows rapid increase compared to the thickness decrease of the downslope flank (Fig. 3). The average WL and WH in Fig. 3 B are approximately 7000 m and 38 m, respectively. The ratio of WL:WH is 180. The average WL and WH exhibited in Fig. 3 C is approximately 1750 m and 15 m, respectively, and the ratio of WL:WH is 117. The size of the sediment wave decreased from a relatively shallow depth to deeper water (Fig. 3). The transition between larger waves (Fig. 3B) versus smaller waves (Fig. 3C) appeared to be rather abrupt, just the site of the slope break. The wave fields are commonly neighboring with the channel or canyon (Figs. 3 and 4). The wave size directly depends on distance to the channel transporting the materials of the Dongsha Platform to deep water, e.g., the closer to the channel, the larger the wave (Fig. 4B) because after spillover, the high-power flow carries more load to form larger sedimentary wave field at close channel, and then as the distance to channel increases, the slope becomes gradually gentle, and the flow has lower power and carries less load, resulting a smaller wave field. The base of the wave field was identified, which also shows that the wave grow along with the neighboring channel or canyon.

The three piston cores were all located in the T-1 wave field (Figs. 2B and 5) and the water depth of the three cores gradually deepened (Fig. 2B). The cores generally contained several sand layers, which were especially evident in core HD-77, where the percentage of sand was up to 72.1%, with a thickness of a single sand layer exceeding 1.5 m. The percent of

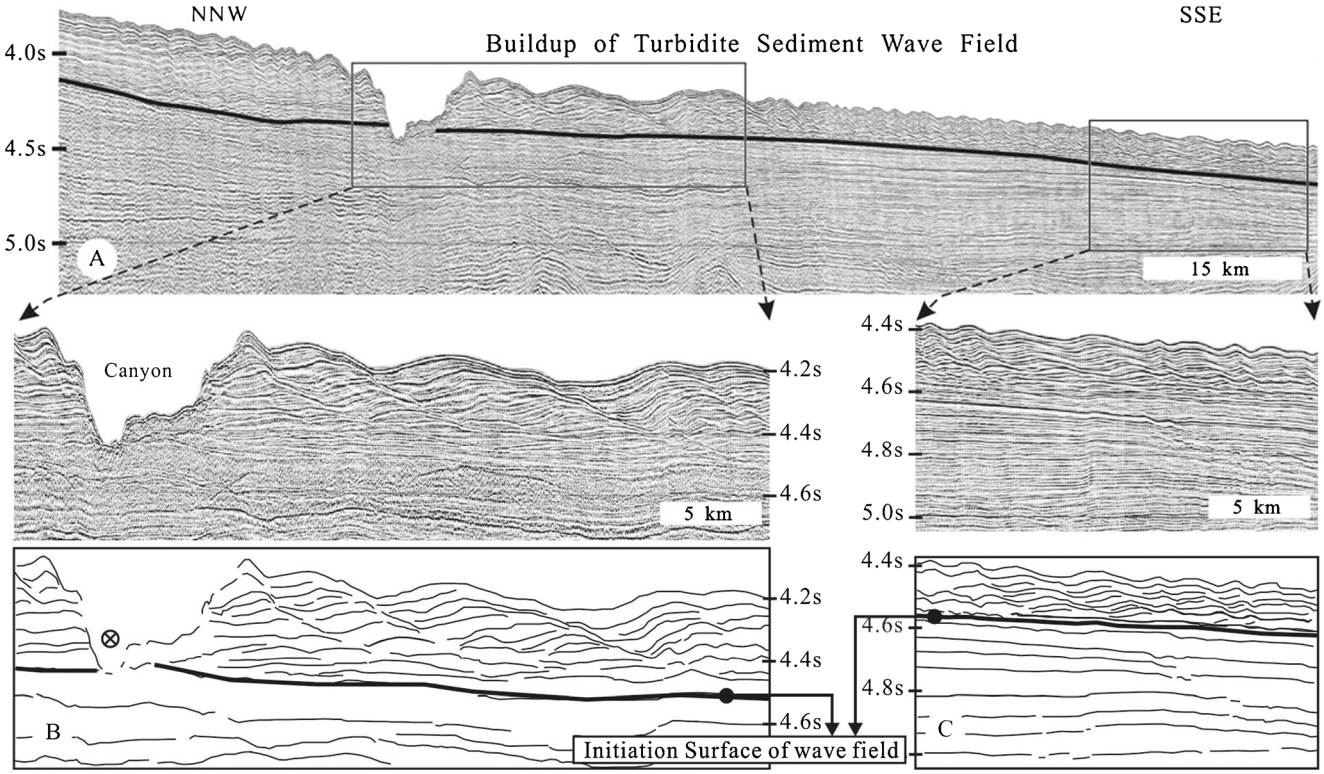

Fig. 3 Seismic profile illustrating the turbidite sediment wave field (T1). The waveform and size are changing evidently and the dynamics of the gravity flow changes dramatically during and along the path of the flow

sand and silt was up to 94.8%. The sand layer was structureless and had several erosive features, such as scours. The median grain size of the entire core HD-77 was between 5.4 and 69.8 μm. The coarse and fine layers alternate rapidly, and their average grain size was 13.6 μm. However, the core HD-207 and HD-200, located upslope and downslope of core HD-77, respectively (Fig. 2B), showed a decrease in sand content and in frequency of alternating coarse and fine layers. The median grain size of core HD-207 was between 5.9 and 20.5 μm, with an average of 8.6 μm. The median grain size of core

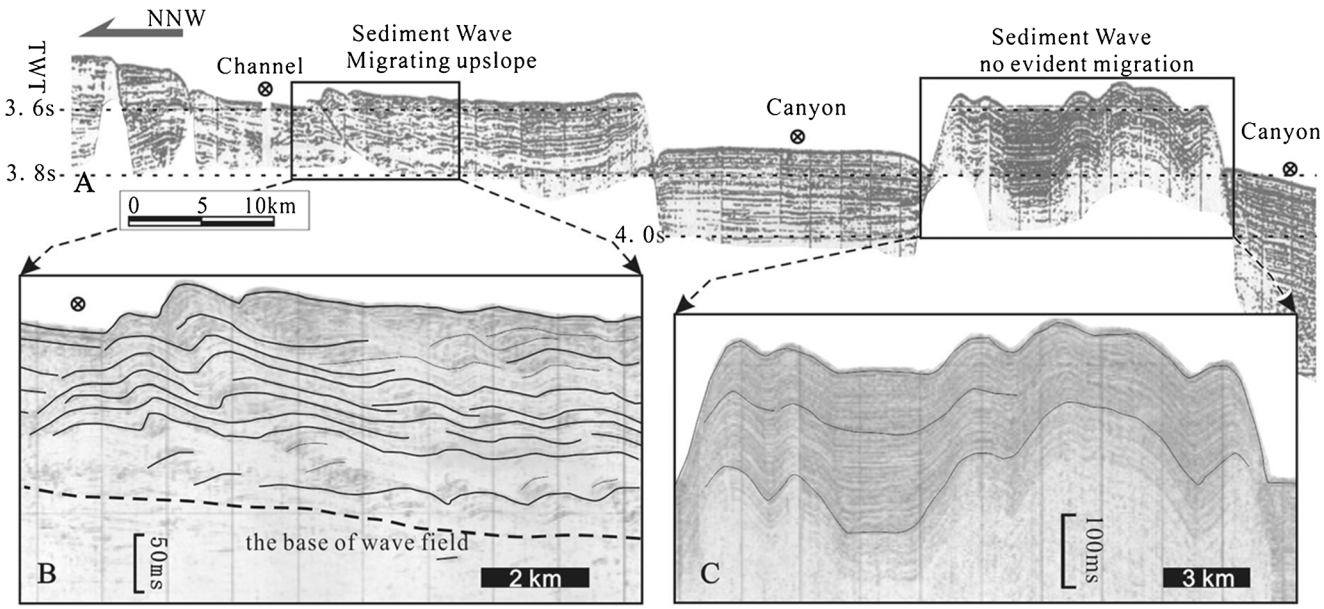

Fig. 4 (A) Single channel seismic profile, illustrating turbidite sediment wave field and some mophosedimentary elements, such as canyons. (B) Note close relationship between form and size of wave, and distance of the wave field to the neighboring channel of a canyon. (C) Sediment waves, with no evident migration and display some symmetry, illustrate the influence of irregular basement on waveform

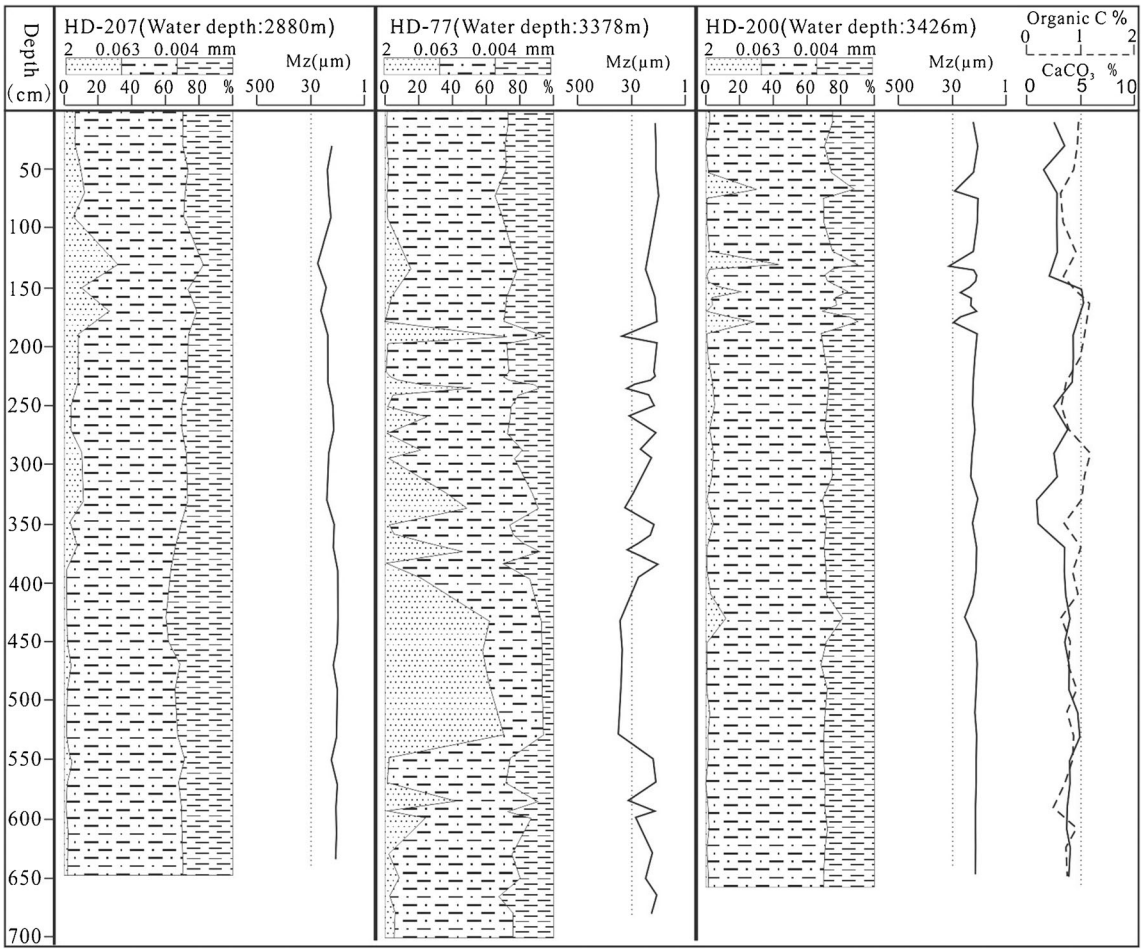

Fig. 5 Three piston cores on the slope of the northern margin, illustrating grain size, average grain size, content of organic carbon, and $CaCO_3$. They all are located on the western flank of the Taiwan Shoal Slope, where gravity flows dominate because of the strong uplift and immense denudation accompanying the Taiwan Orogeny. Each cores generally contains several sand layers, whereas the differences in composition of sand layers reflect distance of core to canyon. Note the difference of $CaCO_3$ content. See the location of cores in Fig. 2 B

HD-200 was between 6.6 and 38.0 μm, with an average of 9.2 μm. Both cores were finer-grained than the core HD-77. The distribution of grain sizes in the three cores, taken at different water depths, is probably related to the relative location of each core with respect to a channel (or canyon). In addition, the $CaCO_3$ content of core HD-200 was between 0.96 and 5.32%, with an average of 3.52% (Fig. 5).

Origin

As mentioned above, these wave fields demonstrate the upslope migration. The ratios of WL:WH of three wave fields are very large (Table 2). Furthermore, the cores show a higher content of sand, a decrease of grain size from upslope to downslope, and a lower content of $CaCO_3$, which also suggest a turbidite flow origin rather than a contour current.

At the site of the slope break, the abrupt characteristic between larger waves (Fig. 3B) versus smaller waves (Fig. 3C) reveals the shifting of the dynamics of the turbidite flows. In addition, the bedforms are associated with the channel or canyon, which acts as the transporting passageway for the flow. The channel seems to grow along with the wave field, which may indicate a close relationship between these entities (Fig. 4B). Such phenomena are the typical feature of the turbidite flows, and have been reported in the Toyama Deep-Sea Channel system in the Japan Sea (Nakajima et al. 1998) and other areas of the world mentioned above. Spillover is an important process of channelized flows especially for those flowing in channels with meanders. Flow stripping or inertial spillover can construct not only the levees along both flanks of the channel, but also the sediment wave fields in those levees (Savoye et al. 1993; Nakajima et al. 1998; Migeon et al. 2000; Normark et al. 2002; Migeon et al. 2004; Casalbore et al. 2018). After spillover, the currents become shallow and slow quickly because the topography is non-confined and corresponds to the dispersal of currents, which changes the trends of waveforms (Lee et al. 2002). In cores, the sand layer was structureless and had several erosive features, such as scours,

which indicates the deposition of debris flows actively sweeping the Taiwan Shoal slope.

The wave fields T-1 and T-4 constituted a whole turbidite sediment wave fields. The initiation of T-1 and T4 was closely controlled by the initiation of the Taiwan orogeny and the unique nature of the southward-propagating focus of the collision (Damuth 1979; Wang et al. 2008). The Taiwan orogeny exhibits the most spectacular physiography in the island-arc belt around the Pacific, and has provided enough and favorable conditions of an immense supply of sedimentary material for the active gravity flow areas acting within the northern Luzon Trough, and potentially has led to the development of the turbidite sediment wave field of possible Quaternary age (Lin et al. 2003). Additionally, the collision propagated southward (Davies et al. 2001; Suppe 1984), and the focus of collision is located presently in the Hengchun Peninsula. Thus, the physical denudation rate of Taiwan is the largest in the world, and it is up to 1300 mg/cm^2 year. Specifically, southern Taiwan can attain the 1796 mg/cm^2 year (Li 1976). The neighboring Kaoping Shelf is a narrow, shallow, and high gradient shelf (20 km wide, 80 m deep and 5 m/km) (Yu and Chiang 1997). Kaoping canyon transects the shelf and links with the Kaoping Hsi River. The enormous clastic input from the Central Range is transported through the Kaoping Hsi River and Kaoping canyon to deep water environments through gravity flows. In fact, the anatomy of the initiation and development of turbidite sediment wave fields T-1 and T-4 can also reveal detailed processes and geological history of arc-continent collision between Luzon Arc and the Eurasion Continent.

Contourite sediment wave fields

Characteristics

Likewise, three similar sediment wave fields were recognized in the northern South China Sea (Table 2), and are shown as three red areas (C-1, C-2, and C-3) in Fig. 2. The area of these three fields was smaller than the turbidite sediment wave fields. In particular, the fields C-1 and C-2 were only 263 km^2 and 240 km^2, respectively.

The sediment wave field C-2 is the shape of the string, and approximately parallel to the trend of the slope, located at the transition of the middle to lower slope (Figs. 2C and 6).

An erosion field is adjoining this wave field in deeper water, and exhibiting various erosive characteristics that included two linear and transverse troughs of 73 m and 120 m depth and 3150 m and 3500 m width, respectively. Moreover, there are some erosive scarps and many small-scale scours or furrows (Fig. 6).

The seismic profile (C-2) of Fig. 6 A is located in the eastern part of the Shenhu area. As illustrated, the average WL and WH a large wave were up to 2250 m and 95 m, respectively, and the ratio of WL:WH was about 23. In contrast, the average WL and WH of the small scale wave were 49 m and 1386 m, respectively, and the ratio of WL:WH was about 28. Their ratios of WL:WH are much smaller than those of turbidite sediment wave fields (Table 2). Furthermore, the sediment wave displayed similar features of upslope migration. Among the layers within the wave-like sedimentary sequence, the discontinuities also were exhibited.

The two piston cores illustrated in Fig. 8 were located in these sediment wave fields. Specifically, the core HS-35 was in the sheeted depositional area of the wave field C-2, and the core HS-60 was located within the wave field C-2 (Fig. 2C). Compared with those cores dominated by turbidite flows, the number of sand layers and the content of sand in these wave field areas decreased dramatically. The sand content of core HS-35 was between 0.48 and 6.37%, and the average was only 2.18%. The core HS-60 had sand content ranging from 0.91 to 19.64%, with an average of 4.97%. Compared with the core HS-35, the relatively high content of coarse grain sizes in the core HS-60 was the result of stronger washing and winnowing by the contour current. The curve reflecting median grain size and composition of cores HS-35 and HS-60 was smooth, with the Mz ranging from 4.9 to 8.1 μm and 4.7 to 14.3 μm, respectively. The content of $CaCO_3$ in core HS-35 was between 13.42 and 30.97%, and the average was 22.89%, whereas core HS-60 had a $CaCO_3$ content between 13.25 and 31.6%, with an average of 20.58%.

Origin

The characteristics of these fields were very different from contourite sediment wave fields of thousands or even tens of thousands of square kilometers in open ocean regions, such as the Northern Atlantic (Von Lom-Keil et al. 2002; Masson et al. 2002), and can be attributed to the unique circulation of the deep water contour current in the South China Sea (Wang 2007; Chen et al. 2017).

The sediment wave fields C-1 and C-2 are approximately parallel to the slope, revealing the properties of contourite sediment wave fields. Evidently, the erosive troughs in these sediment wave fields are different from the longitude canyon (or channel) of typical turbidite flows with respect to their trend in relation to slope. There are no deep water canyons or channels in the detailed topographic maps of the area, and it also lacks other characteristics of gravity deformation or flows, such as slides, slumps, and debris flows. Several relatively small u-shaped erosive scours in such wave field have developed on the present seabed, which may be indicative of a switch or migration of the core of current (Stow et al. 2002; Baldwin et al. 2017). Thus, the wave fields, erosive fields, and depositional wedges constitute a complete depositional system of bottom currents (Figs. 6 and 7). Internal waves in the deep ocean also can form sediment wave fields of similar

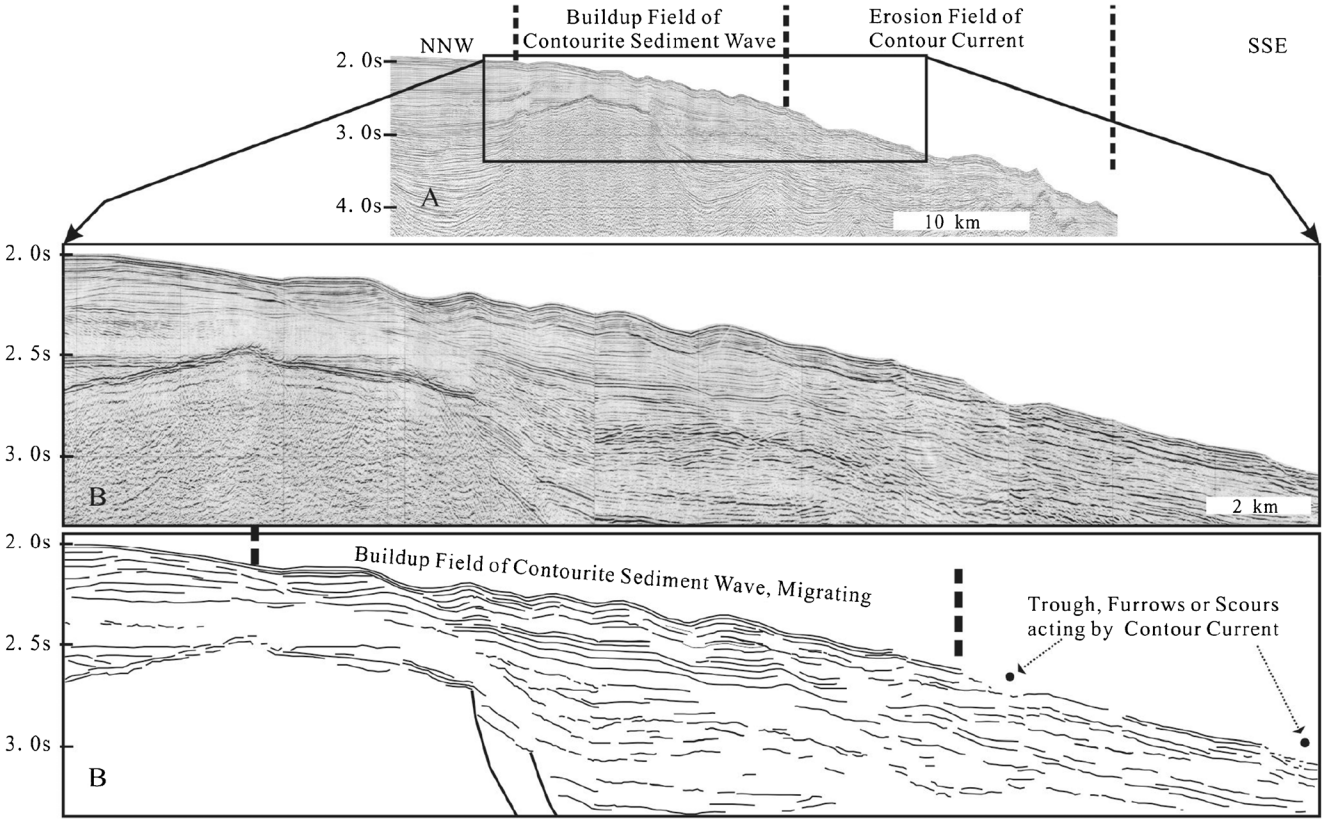

Fig. 6 (A) Seismic profile illustrating the erosion and corresponding sedimentation of the bottom current (C-2), with the migration and stratal architecture of the wave and scour of the bottom shown. (B) The extent of different fields. See the location of cores in Fig. 2 C

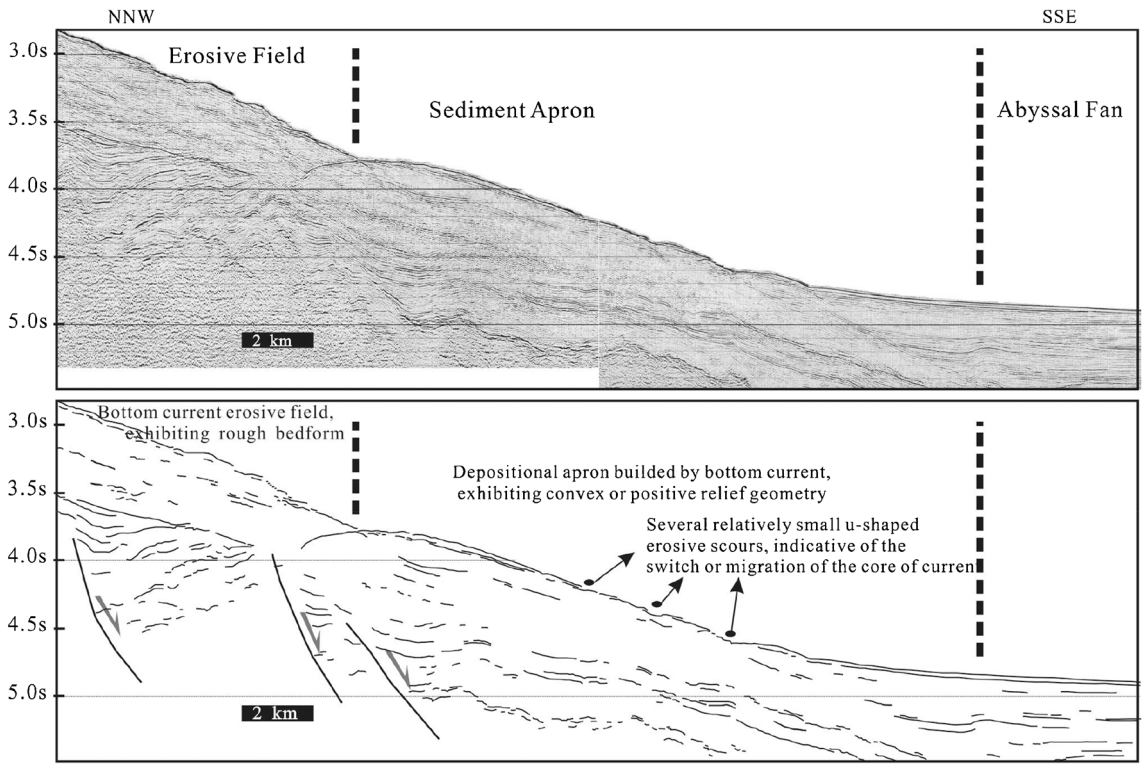

Fig. 7 Depositional wedge illustrating convex or positive relief, built by bottom currents. Note several relatively small u-shaped erosive scours under apron buildups

characteristics. The distributions of wave fields C-1 and C-3 were directly related to the abrupt changing topography which was eroded by the accelerating bottom current and maybe the source of the confined areal extent of contourite sediment wave fields. The above features of these sediment wave fields indicated the origin of bottom currents referring to the diagnostic criterion of wave origin (Table 1). The buildup of the contourite sediment waves and adjoining erosive fields together constitute a whole system, including erosion, dispersion, and transport, and deposition.

In the piston cores, compared with those cores dominated by turbidite flows, the number of sand layers and the content of sand in these wave field areas decreased dramatically, resulting in finer grain size. The $CaCO_3$ contents are greater than that in cores from turbidite sediment wave field (Figs. 5 and 8). Evidently, the sand content, grain size distribution, and content of $CaCO_3$ are all in agreement with their bottom current origin.

Sediment waves formed by bottom currents can help us reveal the onset, circulation, and evolution of related deep water currents in the South China Sea. The SCS has a complex energetic circulation. In such circumstances, the study of contourites and deep water circulation in the SCS is crucial.

Wang (2007) suggested that the sediment wave fields formed by bottom currents in the northern deep water environment of the SCS have developed since the late Miocene, and their origin, location, and distribution have been controlled by the tectonism of the adjoining region and/or palaeoceanography, due to interaction of bathymetry and currents. In return, the evolution of contourite sediment waves, especially the initiation of such waves, usually implies abundant information on tectonism, paleoceanography, and paleoclimatology. Marginal seas such as the SCS respond more sensitively to such events (Wang 1999). The contourite sediment wave field C-2 is closely related to the expansion of the east Antarctic ice sheet (Zachos et al. 2001) during the Late

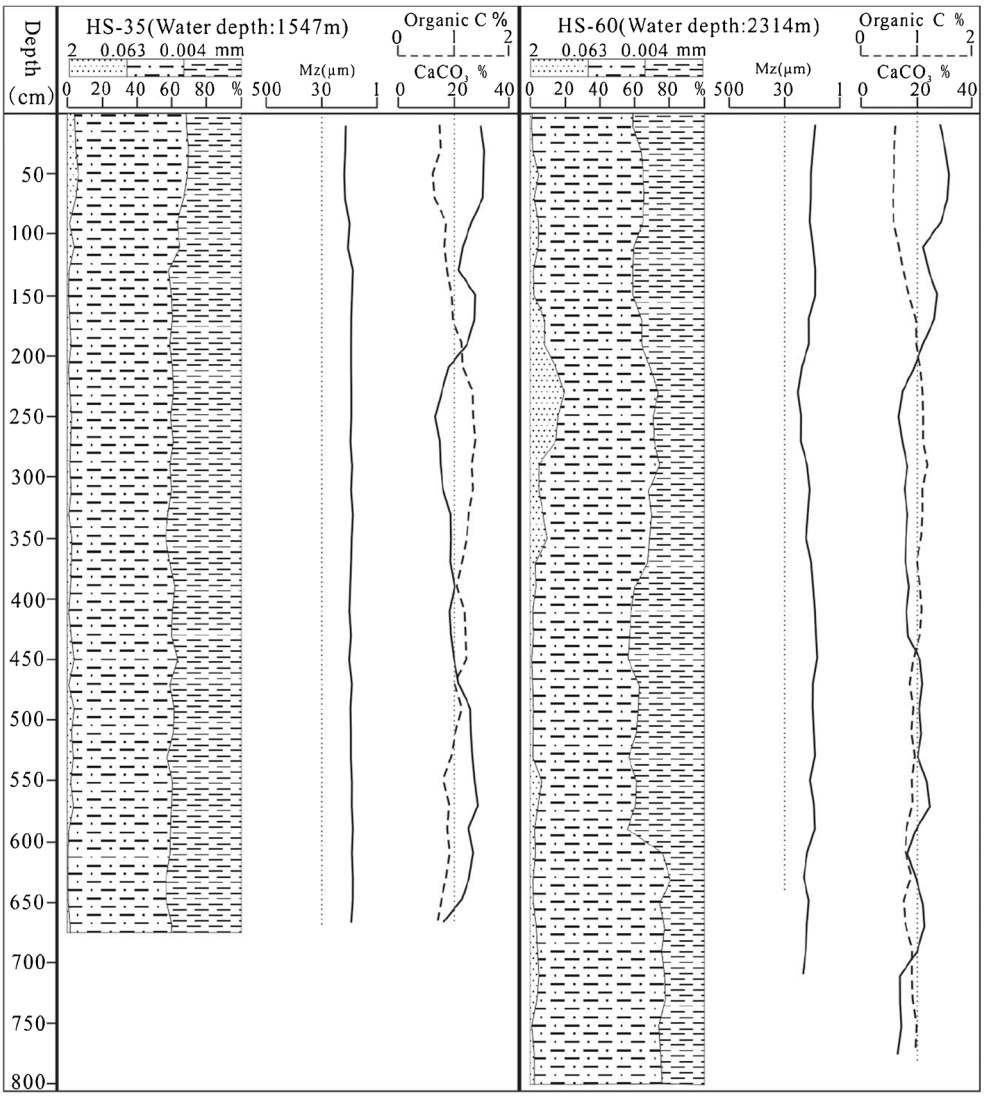

Fig. 8 Two piston cores on the slope of the northern margin, illustrating grain size, average grain size, content of organic carbon, and $CaCO_3$. Both cores of the deep water area of the ShenHu Slope were taken where bottom currents dominate. Core HS-60 is located at the margin of the contourite sediment wave field. Note the lower content of sand and the similarity of content of $CaCO_3$ between both cores. See the location of cores in Fig. 2 C

Miocene, about 14–10 Ma, which greatly increased thermohaline circulation and allowed bottom currents to infiltrate the semi-closed SCS. This pattern started the unique circulation of bottom currents in the South China Sea (Wang 2007). These contour currents eventually developed the sedimentation and erosion patterns measured in this study.

Deformation-origin, wave-like sediment wave fields

Characteristics

In our study area, two wave fields were recognized (two purple regions in Fig. 2 and Table 2). Their sizes are greatly different. The wave fields G-1 and G-2 were 1940 km^2 and 259 km^2, respectively. For the wave field G-1, the WL of the downslope flank was between 0.71 and 1.37 km, while the WL of the upslope flank was from 0.36 to 0.64 km, which reflects unsymmetrical waveforms. In addition, the WH was between 17.16 and 68.16 m. Furthermore, the variation of wave parameters had no regularity compared to those of turbidite or contourite waves. One common feature was their close proximity to the canyon. The field G-2 was on the southwestern flank of Dongsha Island, and also neighbored one huge canyon. The field G-1 was located on the upper and middle slope adjacent to one unnamed canyon and the immense Zhujiang Valley. The field G-1 developed similar 5–6 high-angle reflections that are tilted to the sea and have steep top and gentle bottom (Fig. 9). These reflections extend to the wave trough to top and gradually slide on the same surface at the base of the waves, which can be called "decollement" surface. Besides these features, a sediment drift exists below the "decollement" surface (Fig. 9). Waveforms were long and smooth on the downslope flank, and short and steep on the upslope flank.

Origin

The seismic profile located on the upper slope of the Shenhu region illustrates the close relation of waves with the canyon (Fig. 9). Frequent flushes of gravity flows in canyons can impact levees of canyons and neighboring areas, and furthermore, they are more apt to induce creeping of unconsolidated strata under such steep environment conditions. On the one hand, the canyon makes a relief steeper locally, which is conducive to gravity sliding. On the other hand, the impact of intermittent gravity flow can play the role of internal inducement of gravity action.

In addition, one typical characteristic of these two sediment wave fields developed the "decollement" surface and a sediment drift below this surface. The wave troughs seemed to correspond to those sliding surfaces, which imply their origin as gravity deformation features (Table 1). For the shallowly buried and unconsolidated strata, they easily suffer some deformation and form geometries of wave-like deposits

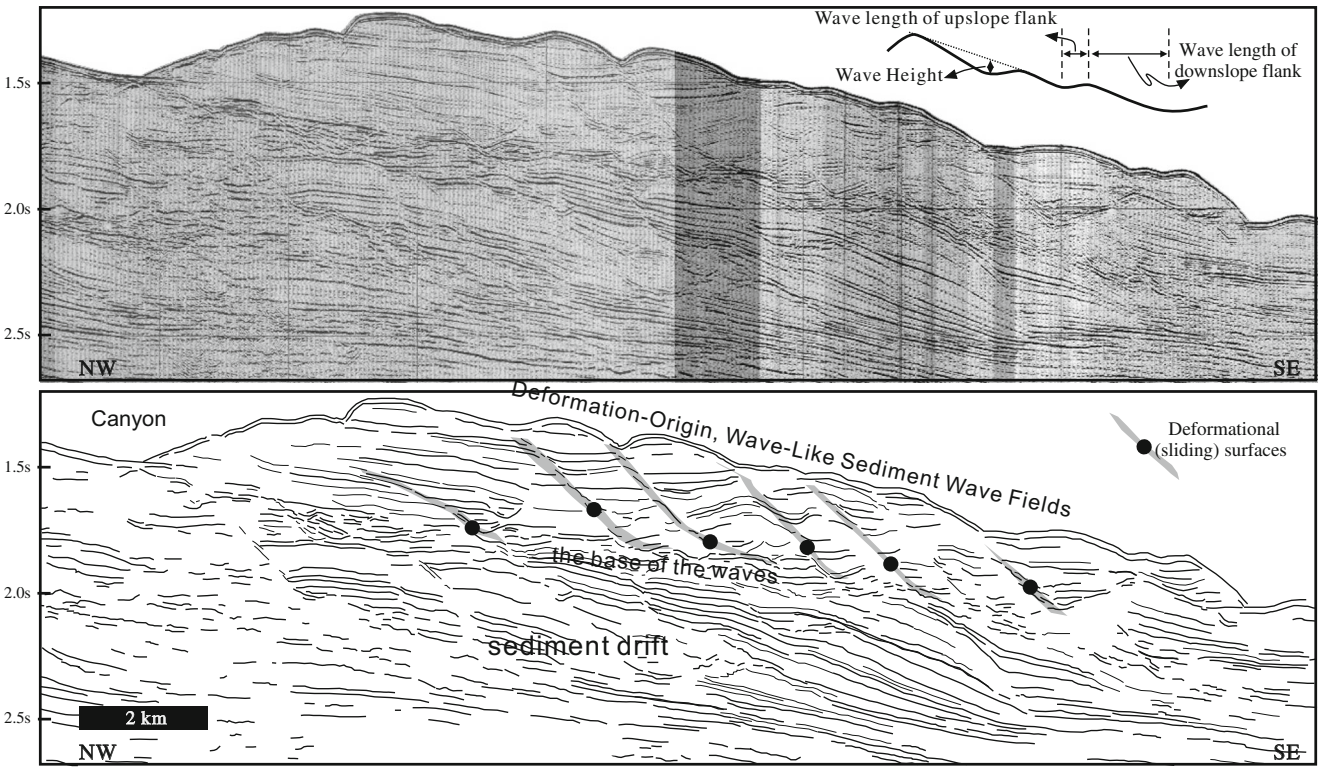

Fig. 9 Seismic profile illustrating the deformation-origin, wave-like sediment wave field (G1), and accompanying other information, including sliding surface, the base of wave fields, and buried drift below the base. Note the neighboring related canyon

(O'Leary and Laine 1996; Lee and Chough 2001; Wynn and Stow 2002; Lee et al. 2002).

Multi-processes sediment wave fields

Characteristics

One unique sediment wave field was recognized in the northern SCS (Table 2), and is shown as blue area (W-1) in Fig. 2. The wave field W-1 was located on the right flank of the Zhujiang Valley. Compared with the wave fields formed by turbidite flow, bottom current, and gravity-induced deformation, the wave field W-1 displayed a smooth and rounded morphology, and was more symmetrical, and have not evident migration direction (Fig. 10). The WL and WH varied greatly, and were between 1.8 and 4.2 km, and 12 and 45 m, respectively (Fig. 10).

Origin

On the northern slope of the SCS, there are some wave fields which cannot be classified into the three types mentioned above. Considering the physiographical site, geological setting, geomorphological characteristics, and hydrodynamics, the wave fields can be formed by the interaction of multiple processes in deep water environments.

Because the W-1 was close the Zhujiang Valley, it was readily impacted by the overspilling of turbidite flows caused by Coriolis effects. The turbidite flows constitute one of the origins of wave field W-1. In addition, the west area of W-1 presents a spectacular contourite sediment wave field termed C-2. Because of variations of slope trends and the convex topography, the W-1 was strongly overprinted by contour currents. Thus, at the site of wave W-1, there were two processes: overflowing of turbidite flows and sweeping of bottom currents (Fig. 10) that is the W-1 formed by the interaction of

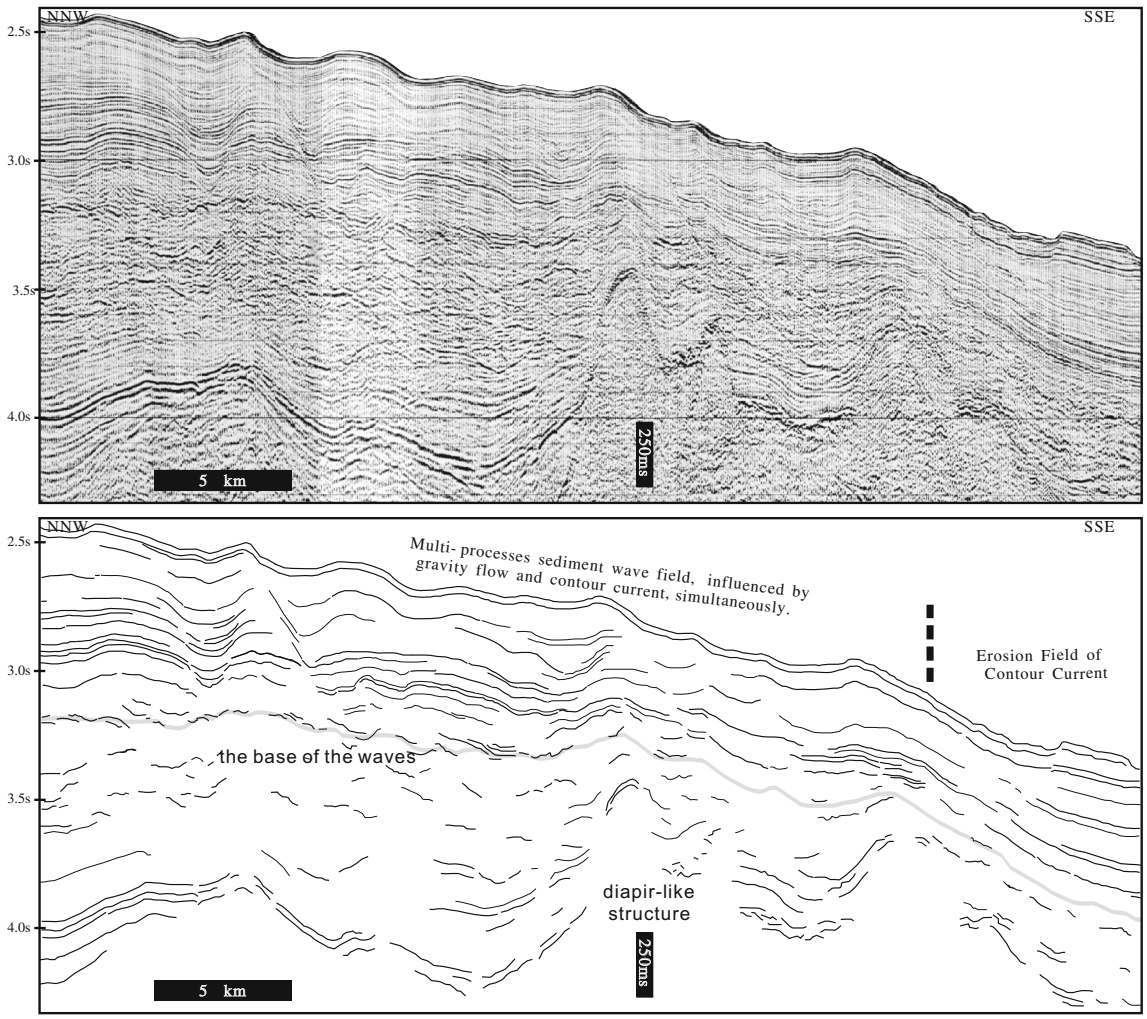

Fig. 10 Seismic profile illustrating the sediment wave of the multi-origin of gravity flow and bottom current. The waveform has no evident migration and appears to have some relation with the underlying basement diapir. The cores in the wave field can illustrate its genesis and the location of cores can be seen in Fig. 2 C

gravity flows and bottom currents. The differences in migrating trends of the turbidite flow and bottom current processes resulted in no evident migration trend for the wave field W-1.

Additionally, the northern slope of the SCS exhibited active volcanic diapirism and faulting in our study area which, in turn, influences the geomorphology and dynamics of depositional processes. The highly varying relief formed by tectonic movement enhanced sedimentation and the initiation and development of the wave field. This is evident in Fig. 10, where the topography formed by the volcanic diapir is related to the developing waveform.

Conclusions

The northern slope of the SCS provides an example of sediment waves from one enclosed and low-latitude marginal sea. There is a continuum of waves developed on the northern slope simultaneously. The conclusions are as follows:

Three sediment wave fields are neighboring to the channel or canyon, decrease for the size from a shallow depth to deeper water, and show the up-current migration. Furthermore, they have a greater content of sand (with no structure), a decrease of grain size from upslope to downslope, and a lower content of $CaCO_3$ in piston cores. These characteristics reveal the origin of turbidite flow.

Three sediment wave fields are parallel to the trend of the slope, develop small-scale erosive troughs, scours or furrows, and depositional convex aprons on the downslope of the erosive field. In the piston cores, they have a lower content of sand, a fine grain size, and a greater content of $CaCO_3$. These characteristics indicate the origin of bottom current.

Two sediment wave fields are adjacent to the canyon, and develop several sliding surfaces corresponding to wave troughs, wave variation of no regularity, implying their origin as gravity deformation. One sediment wave field showed a more symmetrical waveform, displayed a smooth and rounded morphology, and has not evident migration direction, which results from the interaction of turbidite flows and bottom currents.

Every sediment wave field has a unique process of formation, which usually involves a complex interaction between geomorphology, tectonic setting of neighboring area, and oceanographic conditions of the SCS.

Acknowledgements Thanks are extended to D. Van Rooij of Ghent University and one anonymous reviewer for their very detailed comments. We also are grateful to Mr. Mike Wareing (MInstLMe) and Daniele for their comments, text, and grammar of this article.

Declarations

Conflict of interest The authors declare that they have no competing interests.

References

Alexandre N, Calvin CD, Cartigny MJB (2019) The influence of turbidity currents and contour currents on the distribution of deep-water sediment waves offshore eastern Canada. Sedimentology 66(5):1746–1767

Baldwin KE, Mountain GS, Rosenthal Y (2017) Sediment waves in the Caroline Basin suggest evidence for Miocene shifts in bottom water flow in the western equatorial Pacific. Mar Geol 417:194–202

Berndt C, Cattaneo A, Szuman M, Trincardi F, Masson D (2006) Sedimentary structures offshore Ortona, Adriatic Sea—deformation or sediment waves? Mar Geol 234:261–270

Casalbore D, Romagnoli C, Bosman A, Chiocci FL (2014) Large-scale seafloor waveforms on the flanks of insular volcanoes (Aeolian Archipelago, Italy), with inferences about their origin. Mar Geol 355:318–329

Casalbore D, Falcini F, Martorelli E, Morelli E, Bosman A, Calarco M, Chiocci FL (2018) Characterization of overbanking features on the lower reach of the Gioia-Mesima canyon-channel system (southern Tyrrhenian Sea) through integration of morpho-stratigraphic data and physical modelling. Prog Oceanogr 169:66–78

Casalbore D, Clare MA, Pope EL, Quartau R, Bosman A, Chiocci FL et al (2020) Bedforms on the submarine flanks of insular volcanoes: new insights gained from high resolution seafloor surveys. Sedimentology.

Cattaneo A, Correggiari A, Marsset T, Thomas Y, Marsset B, Trincardi F (2004) Seafloor undulation pattern on the Adriatic shelf and comparison to deep-water sediment waves. Mar Geol 213:121–148

Centurioni LR, Niiler PP, Lee DK (2004) Observations of inflow of Philippine Sea surface water into the South China Sea through the Luzon Strait. J Phys Oceanogr 34:113–121

Chang YT, Hsu WL, Tai JH, Tang TY, Chang MH, Chao SY (2010) Cold deep water in the South China Sea. J Oceanogr 66:183–190

Chen H, Zhan W, Li L, Wen M (2017) Occurrence of submarine canyons, sediment waves and mass movements along the northern continental slope of the South China Sea. J Earth Syst Sci 126(5):73. https://doi.org/10.1007/s12040-017-0844-9

Damuth JE (1979) Migrating sediment waves created by turbidity currents in the northern South China Basin. Geology 7:520–523

Davies R, Cartwright J, Pike J, Line C (2001) Early Oligocene initiation of North Atlantic Deep Water formation. Nature 410:917–920

Droghei R, Falcini F, Casalbore D, Martorelli E, Mosetti R, Sannino G, Chiocci FL (2016) The role of Internal Solitary Waves on deep-water sedimentary processes: the case of up-slope migrating sediment waves off the Messina Strait. Sci Rep 6:36376

Ercilla G, Alonso B, Wynn RB, Baraza J (2002a) Turbidity current sediment waves on irregular slopes: observations from the Orinoco sediment-wave field. Mar Geol 192:171–187

Ercilla G, Wynn RB, Alonso B, Baraza J (2002b) Initiation and evolution of turbidity current sediment waves in the Magdalena turbidite system. Mar Geol 192:153–169

Ercilla G, Juan C, Perianez R, Abril BA, Estrada F, Casas D, Vázquez JT, d'Acremont E, Gorini C, Valencia J (2019) Influence of alongslope processes on modern turbidite systems and canyons in the Alboran Sea (southwestern Mediterranean). Deep-sea Res PT I 144:1–16

Faugéres JC, Stow DAV (1993) Bottom-current controlled sedimentation: a synthesis of the contourite problem. Sediment Geol 82:287–297

Faugères JC, Stow DAV, Imbert P, Viana A (1999) Seismic features diagnostic of contourite drifts. Mar Geol 162:1–38

Faugères JC, Gonthier E, Mulder T, Kenyon N, Cirac P, Griboulard R, Bernè S, Lesuavé R (2002) Multi-process generated sediment waves on the Landes Plateau (Bay of Biscay, North Atlantic). Mar Geol 182:279–302

Fildani A, Normark WR, Kostic S, Parker G (2006) Channel formation by flow stripping: Large-scale scour features along the Monterey East Channel and their relation to sediment waves. Sedimentology 53(6):1265–1287

Gardner JV, Prior DB, Field ME (1999) Humboldt slide: a large shear-dominated retrogressive slope failure. Mar Geol 154:323–338

Gong C, Wang Y, Peng X (2012) Sediment waves on the South China Sea Slope off southwestern Taiwan: implications for the intrusion of the Northern Pacific Deep Water into the South China Sea. Mar Pet Geol 32(1):95–109

Guan BX (1978) The warm current in the South China Sea. Oceanologia et Limnologia Sinica 9:117–127 (in Chinese)

Habgood EL, Kenyon NH, Masson DG, Akhmetzhanov A, Weaver PPE, Gardner J, Mulder T (2003) Deep-water sediment wave fields, bottom current sand channels and gravity flow channel-lobe systems: Gulf of Cadiz, NE Atlantic. Sedimentology 50:483–510

Ho CS (1988) An introduction to the geology of Taiwan: explanatory text for geologic map of Taiwan. Republic of China, Taipei, Taiwan, Ministry of Economic Affairs, 192p

Howe JA (1996) Turbidite and Contourite sediment waves in the northern Rockall Trough, North Atlantic Ocean. Sedimentology 43:219–234

Huang CY, Lin CW, Wang TK, Chang CP, Yuan PB (2000) Geodynamic processes of Taiwan arc–continent collision and comparison with analogs in Timor, Papua New Guinea, Urals and Corsica. Tectonophysics 325:1–21

Jallet L, Giresse P (2005) Construction of the Pyreneo-Languedocian Sedimentary Ridge and associated sediment waves in the deep western Gulf of Lions (Western Mediterranean). Mar Pet Geol 22:865–888

Jorry SJ, Isabelle J, Emmanuel L, Ricardo SJ, Savoye B (2011) Turbiditic levee deposition in response to climate changes: the Var Sedimentary Ridge (Ligurian Sea). Mar Geol 279(1–4):148–161

Kenyon NH, Belderson RH, Stride AH (1978) Channels, canyons and slump folds on the continental slope between South-West Ireland and Spain. Oceanol Acta 1:369–380

Khripounoff A, Vangriesheim A, Babonneau N, Crassous P, Dennielou B, Savoye B (2003) Direct observation of intense turbidity current activity in the Zaire submarine valley at 4000 m water depth. Mar Geol 194:151–158

Klauckea I, Massona DG, Kenyona NH, Gardner JV (2004) Sedimentary processes of the lower Monterey Fan channel and channel-mouth lobe. Mar Geol 206:181–198

Knutz PC, Jones EJW, Howe JA, Weering TJC, Stow DAV (2002) Wave-form sheeted contourite drift on the Barra Fan, NW UK continental margin. In: DAV S, Pudsey CJ, Howe JA, Faugères JC, Viana AR (eds) Deep-water contourite systems: modern drifts and ancient seires, seismic and sedimentary characteristics, vol 22. Geological Society, London, Memoirs, pp 85–97

Lan J, Zhang NN, Wang Y (2013) On the dynamics of the South China Sea deep circulation. J Geophys Res Ocean 118(3):1206–1210

Lee HJ, Baraza J (1999) Geotechnical characteristics and slope stability in the Gulf of Cadiz. Mar Geol 155:173–190

Lee SH, Chough SK (2001) High-resolution (2-7 kHz) acoustic and geometric characters of submarine creep deposits in the South Korea Plateau, East Sea. Sedimentology 48:629–644

Lee HJ, Syvitski JPM, Parker G, Orange D, Locat J, Hutton EWH, Imran J (2002) Distinguishing sediment waves from slope failure deposits: field examples, including the 'Humboldt slide', and modelling results. Mar Geol 192:79–104

Li YH (1976) Denudation of Taiwan island since the Pliocene Epoch. Geology 4:105–107

Li L, Nowlin WD, Su JL (1998) Anticyclonic rings from the Kuroshio in the South China Sea. Deep-Sea Res 145:1469–1482

Lin AT, Watts AB, Hesselbo SP (2003) Cenozoic stratigraphy and subsidence history of the south China Sea margin in the Taiwan region. Basin Res 15:453–478

Liu XB, Su JL (1992) A reduced gravity model of the circulation in the South China Sea. Oceanologia et Limnologia Sinica 23:167–174 (in Chinese)

Llave E, Schönfeld J, Hernández-Molina FJ, Mulder T, Somoza L, Díaz del Río V, Sánchez-Almazo I (2006) High-resolution stratigraphy of the Mediterranean outflow contourite system in the Gulf of Cadiz during the late Pleistocene: The impact of Heinrich events. Mar Geol 227:241–262

MacLachlan SE, Elliott GM, Parson LM (2008) Investigations of the bottom current sculpted margin of Hatton Bank, NE Atlantic. Mar Geol 253:170–184

Maldonado A, Barnolas A, Bohoyo F, Galindo-Zaldívar J, Hernández-Molina FJ, Lobo F, Rodríguez-Fernández J, Somoza L, Vázquez JT (2003) Contourite deposits in the central Scotia Sea: the importance of the Antarctic Circumpolar Current and the Weddell Gyre flows. Palaeogeogr Palaeoclimatol Palaeoecol 198:187–221

Masson DG, Howe JA, Stoker MS (2002) Bottom-current sediment waves, sediment drifts and contourites in the northern Rockall Trough. Mar Geol 192:215–237

Masson DG, Wynn RB, Bett BJ (2004) Sedimentary environment of the Faroe-Shetland and Faroe Bank Channels, north-east Atlantic, and the use of bedforms as indicators of bottom current velocity in the deep ocean. Sedimentology 51:1207–1241. https://doi.org/10.1111/j.1365-3091.2004.00668.x

McCave IN (2017) Formation of sediment waves by turbidity currents and geostrophic flows: a discussion. Mar Geol 390:89–93

Metzger EJ, Hurlburt H (1996) Coupled dynamics of the South China Sea, Sulu Sea, and the Pacific Ocean. J Geophys Res 101:12331–12352

Metzger EJ, Hurlburt H (2001) The importance of high horizontal resolution and accurate coastline geometry in modeling South China Sea inflow. Geophys Res Lett 28:1059–1062

Migeon S, Savoye B, Faugeres JC (2000) Quaternary development of migrating sediment waves in the Var deep-sea fan: distribution, growth pattern and implication for levee evolution. Sediment Geol 133:265–293

Migeon S, Savoye B, Babonneau N, Spy Andersson FL (2004) Processes of sediment-wave construction along the present Zaire Deep-Sea Meandering Channel: role of meanders and flow stripping. J Sediment Res 74:580–598

Mulder T, Cochonat P (1996) Classification of offshore mass movements. J Sediment Res 66:43–57

Nakajima T, Satoh M, Okamura Y (1998) Channel-levee complexes, terminal deep-sea fan and sediment wave fields associated with the Toyama Deep-Sea Channel system in the Japan Sea. Mar Geol l47: 25–41

Normandeau A, Calvin Campbell D, Cartigny MJB (2019) The influence of turbidity currents and contour currents on the distribution of deep-water sediment waves offshore eastern Canada. Sedimentology 66: 1746–1767

Normark WR, Hess GR, Stow DAV, Bowen AJ (1980) Sediment waves on the Monterey Fan levee: a preliminary physical interpretation. Mar Geol 37:1–18

Normark WR, Piper DJW, Posamentier H, Pirmez C, Migeon S (2002) Variability in form and growth of sediment waves on turbidite channel levees. Mar Geol 192:23–58

O'Leary DW, Laine E (1996) Proposed criteria for recognizing intrastratal deformation features in marine high resolution seismic reflection profiles. Geo-Mar Lett 16:305–312

Petrovic A, Lantzsch H, Schwenk T, Marquardt J, Titschack J, Hanebuth TJJ (2019) Post-LGM upward shift of the Mediterranean Outflow Water recorded in a contourite drift off NW Spain. Mar Geol 407: 334–334

Qu TD (2002) Evidence for water exchange between the South China Sea and the Pacific Ocean through the Luzon Strait. Acta Oceanol Sin 21(2):175–185

Ribó M, Puig P, Muñoz A, Lo Iacono C, Masqué P, Palanques A, Acosta J, Guillén J, Ballesteros M.G (2016a) Morphobathymetric analysis of the large fine-grained sediment waves over the Gulf of Valencia continental slope (NW Mediterranean). Geomorphology 253:22–37.

Ribó M, Puig P, Urgeles R, Van Rooij D, Muñoz A (2016b) Spatio-temporal evolution of sediment waves developed on the Gulf of Valencia margin (NW Mediterranean) during the Plio-Quaternary. Mar Geol 378:276–291

Ribo M, Duran R, Puig P, Van Rooij D, Guillén J, Masqué P (2018) Large sediment waves over the Gulf of Roses upper continental slope (NW Mediterranean). Mar Geol 399:84–96

Savoye B, DJW P, Droz L (1993) Plio-Pleistocene evolution of the Var deep-sea fan off the French Riviera. Mar Pet Geol 10:550–571

Schlüeter P, Uenzelmann-Neben G (2008) Indications for bottom current activity since Eocene times: the climate and ocean gateway archive of the Transkei Basin, South Africa. Glob Planet Chang 60:416–428. https://doi.org/10.1016/j.gloplacha.2007.07.002

Shaw PT (1991) The seasonal variation of the intrusion of the Philippine Sea Water into the South China Sea. Journal of Geophysical Research 96:821–827

South China Sea Institute of Oceanology, Academia Sinica (SCSIO) (1985) Report of the 1979–1982 Multidisciplinary Research Program on the Northern South China Sea, vol II. China Science Press, Beijing, pp 432 (in Chinese)

Stoker MS (1998) Sediment-drift development on the continental margin off NW Britain. In: Stoker MS, Evans D, Cramp A (eds) Geological Processes on Continental Margin: Sedimentation, Mass-Wasting and Stability, vol 129. Geological Society, London, Special Publication, pp 229–254

Stow DAV, Faugères JC, Howe JA, Pudsey CJ, Viana AR (2002) Bottom currents, contourites and deep-sea sediment drifts: current state-of-the-art. In: DAV S, Pudsey CJ, Howe JA, Faugères JC, Viana AR (eds) Deep-water contourite systems: modern drifts and ancient seires, seismic and sedimentary characteristics, vol 22. Geological Society, London, Memoirs, pp 7–20

Su JL (1998) Circulation dynamics of the China Seas: north of 181N. In: Robinson AR, Brink K (eds) The sea, the global coastal ocean: regional studies and syntheses, vol 11. Wiley, New York, pp 483–506

Su J (2004) Overview of the South China Sea circulation and its influence on the coastal physical oceanography outside the Pearl River Estuary. Cont Shelf Res 24:1745–1760

Suppe J (1981) Mechanics of mountain building and metamorphism in Taiwan. Geol. Soc. China Mem 4:67–89

Suppe J (1984) Kinematics of arc-continent collision, flipping of subduction, and back-arc spreading near Taiwan. Geol SocChina 6:21–34

Viana AR, W Jr A, MCV N, Bulhões EM (2007) The economic importance of contourites. In: Viana AR, Rebesco M (eds) Economic and Palaeoceanographic Significance of Contourite Deposits, vol 276. Geological Society, London, Special Publications, pp 1–23

Von Lom-Keil H, Spieß V, Hopfauf V (2002) Fine-grained sediment waves on the western flank of the Zapiola Drift, Argentine Basin: evidence for variations in Late Quaternarybottom flow activity. Mar Geol 192:239–258

Wang P (1999) Response of Western Pacific marginal seas to glacial cycles: paleoceanographic and sedimentological features. Mar Geol 156:5–39

Wang H (2007) Sedimentation processes and its response in deep-water environment of the northern Continental Margin, the South China Sea. Ph.D. thesis, China University of Petroleum, Beijing, 62pp (in Chinese)

Wang P, Wang L, Bian Y, Jian Z (1995) Late Quaternary paleoceanography of the South China Sea: surface circulation and carbonate cycles. Mar Geol 127:145–165

Wang H, Wang Y, Qiu Y, Peng X, Huang Q (2008) Development and its tectonic activity 's origin of turbidity current sediment wave in Manila Trench, the South China Sea. Acta Sedimentologica Sinica 26(1):39–45(in Chinese)

Warratz G, Schwenk T, Voigt I, Bozzano G, Henrich R, Violante R, Lantzsch H (2019) Interaction of a deep-sea current with a blind submarine canyon (Mar del Plata Canyon, Argentina). Mar Geol 417:106002

Wong HK, Lűdmann T, Baranov BV, Konerdieng P, Ion G (2003) Bottom current-controlled sedimentation and mass wasting in the northwestern Sea of Okhotsk. Mar Geol 201:287–305

Wright JD, Miller KG (1996) Control of North Atlantic Deep Water Circulation by the Greenland-Scotland Ridge. Paleoceanography 11:157–170

Wynn RB, Stow DAV (2002) Classification and characterisation of deep-water sediment waves. Mar Geol 192:7–22

Wynn RB, Masson DG, Stow DAV, Weaver PPE (2000) The Northwest African slope apron: a modern analogue for deep-water systems with complex seafloor topography. Mar Pet Geol 17:253–265

Wynn RB, Piper DJW, Gee MJR (2002) Generation and migration of coarse-grained sediment waves in turbidity current channels and channel-lobe transition zones. Mar Geol 192:59–78

Yu HS, Chiang CS (1997) Kaoping Shelf: morphology and tectonic significance. J Asian Earth Sci 15:9–18

Zachos J, Pagani M, Sloan L, Thomas E, Billups K (2001) Trends, rhythms, and aberrations in global climate 65 Ma to present. Science 292:686–693